THERMAL AND ELECTRON-BEAM IRRADIATION EFFECTS ON THE SURFACES OF NIOBIUM FOR RF CAVITY PRODUCTION*

Qing Ma† and Richard A. Rosenberg, Argonne National Laboratory, Argonne, IL 60439

Abstract

Results of a study of thermal and electron-beam irradiation effects on the surfaces of Nb are presented. The samples were prepared by chemical etching methods used in superconducting rf cavity production. For such prepared samples, a layer of Nb_2O_5 covered the surface with some Nb_2O interfacing the Nb metal. Some hydrocarbon species were also found on the surface. Oxidation in air at room temperature will be discussed.

Heating the samples at temperatures from 100 - 300 °C caused reduction of the surface oxide. The reduction rate increased with temperature. Near 100 °C, some Nb_2O_5 reduced and some NbO_x ($x < 2.5$) formed. Near 170 °C, only a little Nb_2O_5 remained after > 70 h. Substantial amounts of NbO_x ($1 \leq x < 2.5$) formed. Heating at these temperatures also caused hydrocarbon decomposition, leaving graphitic carbon on the surface, but had no effect on Nb_2O at the interface. At temperatures > 210 °C, Nb_2O_5 disappeared. Only Nb_2O remained on the surface that exhibited a metallic character. In addition, more than half of the surface carbon reacted with Nb and formed metal carbide. Reaction kinetics will be discussed.

Under 1-keV electron beam irradiation, surface damage occurred. Changes in the secondary electron yield (SEY) were observed and identified to be due to two causes: surface chemical changes and defect creation in the oxide. There was a slope change in the SEY-vs-dose relationship that led to two cross-section values of 4.8×10^{-18} cm^2 and 2.3×10^{-19} cm^2 for the electron/matter interaction. The larger value primarily results from changes in surface chemistry and the smaller one from defect creation.

1. INTRODUCTION

Superconducting rf cavities are used in high-energy particle accelerator facilities to provide high-gradient acceleration. Problems encountered during rf cavity development, such as electron multipacting and the field emission of impurity particulates, have largely been solved and gradients as high as 25 MV/m are now achievable. Recent experiments have shown that baking the cavities near 150 °C improves the cavity performance significantly. The maximum accelerating field can reach as high as 40 MV/m [1,2]. However, the reason for such improvements remains largely unknown. This low temperature should have little effect on the bulk properties of Nb. Therefore the research focus is directed to the possible effect of the baking on surface oxides after chemical or electrochemical processing.

There have been many studies devoted to Nb surfaces. The surface oxidation was studied under various conditions especially at high temperatures (> 300 °C) and at room temperature. Considerable knowledge of the surface oxide chemistry and thermodynamics has been accumulated [3-6]. However, there is a lack of such knowledge in the temperature range from 25 to 300 °C. This knowledge is increasingly in demand as the accelerator community strides to achieve higher accelerating gradients using Nb superconducting rf cavities. We have initiated an effort to study the Nb surfaces with emphasis on the surface chemistry and thermodynamics up to 300 °C and on electron-beam induced surface chemistry. In this paper, results from a study of thermal and electron-beam irradiation effects on Nb surfaces are presented.

2. EXPERIMENTAL

A commercial Nb sheet with 99.99% purity was cut into 1×1 cm^2 squares. The samples were prepared by Buffered Chemical Polishing (BCP) following the procedure used at CERN for rf cavity preparations. For some samples the BCP solutions (1:1:1 and 2:1:1 HPO_3:HNO_3:HF) were cooled down lower than 10 °C, and for others the solutions were used at room temperature. The solution temperature rose about 2 °C during chemical etching. The polished surfaces were rinsed alternatively in deionized water, nitric acid, and hydrofluoric acid. After the BCP treatment, the grain structure was clearly visible.

The samples were analyzed using x-ray photoelectron spectroscopy (XPS) and SEY measurements. The base pressure of the analysis system is 2×10^{-10} Torr. The sample was transferred onto a sample holder, where it could be heated up to 1000 °C or cooled down to –130 °C. The heat source was a W filament located near the back of the sample, and liquid nitrogen was used to cool the sample. A thermocouple attached onto the sample surface measured the temperature.

A VG LEG 200 electron gun was used to perform the electron irradiation. The electron energy was 1 keV. The electron beam current, I_e, and corresponding beam spot size were determined using a Faraday cup. The electron beam was rastered to irradiate the sample surface. The SEY, σ, of a sample surface was monitored as a function of the electron dose. It was measured as a function of impact electron energies using a retarding potential

* The work is supported by the U.S. Department of Energy, Office of Basic Energy Sciences under contract No. W-31-109-ENG-38.

† qingma@aps.anl.gov

method [7] and an electron current density of 6.3 μA/cm^2. Electrons were incident to the surface along the surface normal. The sample current, I_s, was recorded by an electrometer. Therefore, σ is calculated by $(1 - I_s/I_e)$.

For XPS, Mg Kα radiation (1253.6 eV) was used to excite the sample surfaces. A hemispheric electron energy analyzer was used to register the energy distribution curves of emitted photoelectrons. It was operated in the constant-analysis energy mode. Pass energy of 20 eV was used for collecting C-1s, O-1s, and Nd-3d data. The total energy resolution of the system is ~1 eV at the C-1s peak. To follow thermal and electron-beam effects, the XPS data were collected at a take-off angle of 90°, i.e., parallel to the surface normal. Angular-resolved x-ray photoemission spectroscopy measurements and analyses were also performed to estimate the oxide thickness by collecting the photoelectrons at various take-off angles.

The sample temperature rose negligibly upon both x-ray and electron irradiation.

For the XPS data analysis, a Doniach-Sunjic function was used to better simulate the tail produced by many-body events near the Fermi level on the higher binding-energy side of a metal XPS peak. This function contains a singularity factor α. For oxide Nb-3d lines, the α values were set to zero, for which a symmetrical peak shape was assumed. However, the Nb-3d line of Nb_2O exhibited a strong asymmetry, which had to be simulated correctly by employing the α factor. In addition to this, the spin-orbit splitting of Nb 3d was set to be 2.75 eV, and the branching ratio of Nb $3d_{5/2}$ over $3d_{3/2}$ was set to be 1.6.

3. SURFACE OXIDATION IN AIR

Prior to discussion of surface oxidation in air, some findings on the BCP-treated surfaces are summarized. No matter how quickly the etched sample was introduced into vacuum, a layer of oxide and some hydrocarbon species were always found on the sample surface. The oxides were mainly Nb_2O_5. Fluorine was often found on the surfaces, and even phosphorous was found in one case. The surfaces etched at room temperature were not different from those at lower temperatures in terms of surface conditions. However, a broadening of the metal Nb-3d peak was found for some samples etched at room temperature. The broadening disappeared upon heating or storage in UHV for a period of time. Norman studied oxygen dissolution by continuous x-ray diffraction measurements of the basal plane reflection (200) during oxidation of Nb in air at 430 °C [8]. The lattice was expanded by interstitial oxygen, and a line broadening and reduction in peak height were also found. Therefore, the broadening of the metal Nb-3d peak might also be attributable to the interstitial oxygen.

Figure 1 shows the XPS spectra collected on a Nb sample etched at 9 °C and subsequently oxidized in air. Located at 5.4 eV above the metal Nb-3d peak, the Nb_2O_5 Nb-3d peak increased with exposure time. The C-1s and O-1s peaks also increased. The C-1s peak contains a characteristic of hydrocarbon species, while the O-1s peak indicates the existence of oxides and adsorbed O-containing species. The simulation indicated that there was about one monolayer of Nb_2O at the metal/oxide interface, consistent with the results reported in [9]. There might also exist some NbO_2 and NbO, but the analysis was inconclusive.

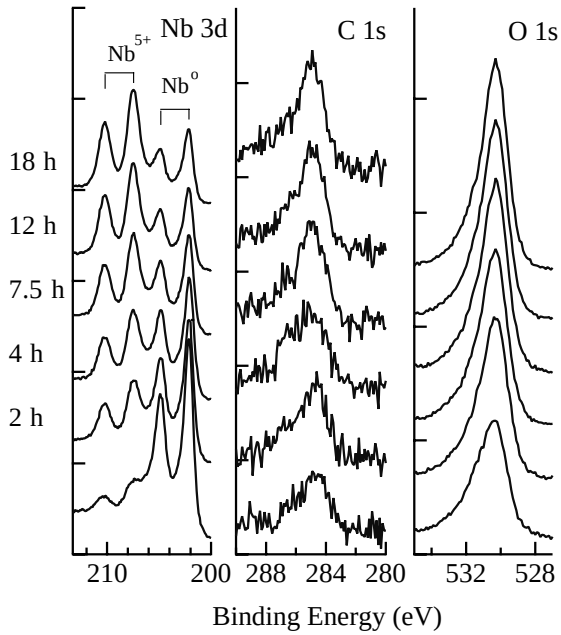

Figure 1: XPS spectra of a Nb sample as a function of time (h) in air. Nb^0: metal and Nb^{5+}: oxide.

Normalization of the metal peaks of the Nb-3d spectra to that of the first spectrum (Fig. 1) produced good matches regarding this peak. Subtracting out the metal Nb-3d peak yielded difference spectra, as presented in Fig. 2. The Nb_2O_5 peak was better resolved and could be fitted using a symmetric Doniach-Sunjic function (α = 0). In addition, the peak associated with Nb_2O was seen at ~0.8 eV above the Nb^0 peak (202.1 eV). This unambiguously confirmed the existence of Nb_2O at the interface. Note that the apparent increase of the Nb_2O intensity with time was due to artifacts from normalization.

The kinetics of oxidation in air at room temperature will be studied in detail in the future. However, some comments may be made based on the data in the inset of Fig. 2. The data are a plot of the Nb_2O_5 thickness vs time. The thickness was determined from the angular-resolved XPS data measured on the sample. The mean free path for Nb_2O_5 was equal to 2 nm at the kinetic energies around Nb 3d (1050 eV). Overall, the relationship of the thickness with time was parabolic, which often indicated a field-assisted oxidation scheme described by Cabrera and Mott [10]. This conclusion is consistent with the results obtained by Grundner and Halbritter despite the differences in the sample preparation method. The detailed data modeling will be presented elsewhere.

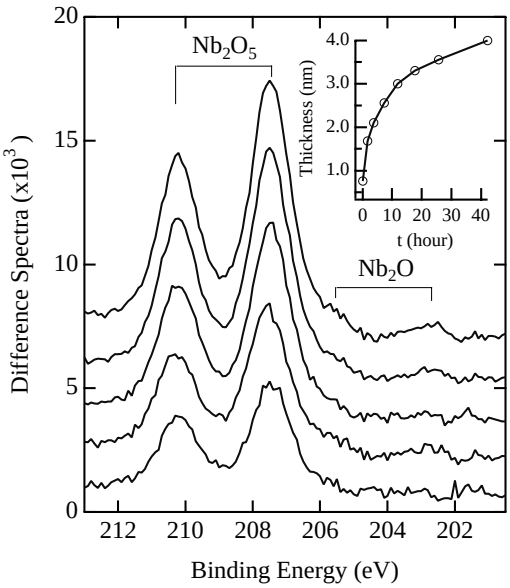

Figure 2: Difference Nb-3d spectra. The inset shows the oxidation kinetics of a parabolic type.

Evidence of field-assisted oxidation of Nb was actually observed on air-oxidized Nb samples by examining peak shifts. Shifts of the oxide Nb-3d and O-1s peaks to higher binding energies relative to the metal Nb-3d peak were found for the samples held in UHV for a period of time or to ones heated moderately. The shifts were as large as 0.2 eV. In either case, desorption events could occur on the surface [4,11]. Such shifts resulted from removal of the surface charges that put the surface at a lower or higher potential, depending on the type of charge, relative to the metal substrate and spectrometer ground. In this case, negative charges existed on the surface. In the field-assisted metal oxidation, an electric field is established between the metal and negative oxygen ions, which are readily produced following oxygen adsorption since oxygen can acquire electrons from the metal due to its high electron affinity. The field will facilitate metal or oxygen ions to migrate in the opposite direction, and thus, accelerate oxidation. As the oxide grows thicker, oxygen ions can be continuously produced via electron tunneling due to the existing field. This field will induce the oxide XPS peaks to shift to lower binding energy but have no effect on the metal peak. Therefore, the observed shifts for air-oxidized Nb samples should be a fingerprint of the existing field across the oxide thickness.

4. THERMAL EFFECT

Surface oxide dissolution into the Nb metal occurred at temperatures > 300 °C. The reaction was described by King *et al*. to be first order and proceeded with an activation energy E_a ~174±6 kJ/mole [3]. The oxide on the Nb surfaces dissolved at even lower temperature [12]. In this section, we present the results of thermal treatment of the surface oxide at temperatures up to 300 °C. Sample heating was carried out by setting the filament current to a value that had been calibrated to achieve the desired temperature. To reach 100 °C to 300 °C, it took typically 30 to 60 min for the sample temperature to reach equilibrium.

Figure 3 shows the Nb-3d spectra measured on Nb samples that were annealed at different temperatures. In each case, changes occurred. Near 100 °C, the Nb_2O_5 peak initially broadened and subsequently decreased. As shown in Fig. 3, the reduction of Nb_2O_5 was incomplete, stopped after nine hours of heating, and some NbO_x formed ($x < 2.5$). During this time, the metal Nb-3d peak increased somewhat, and the O-1s peak (not shown) decreased slightly. The C-1s peak (not shown) shifted from 285 eV to 284.6 eV, and the peak intensity decreased. The peak became more symmetric, as a result of hydrocarbon decomposition. The change in binding energy indicated that most of the carbon on the surface became graphitic. All these changes occurred on a similar time scale and might correlate with one another.

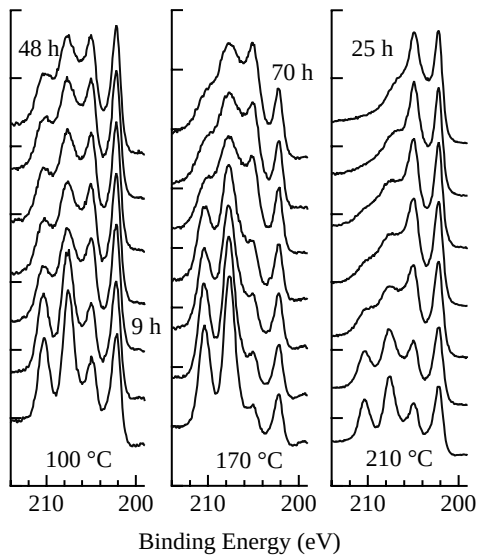

Figure 3: Annealing of the BCP-etched Nb samples at three temperatures. Characteristic times were marked.

At temperatures near 170 °C, the reduction of Nb_2O_5 extended up to ~70 hours, beyond which changes were weak. At this point, only a little Nb_2O_5 remained on the surface (Fig. 3) and substantial amounts of NbO_x ($1 \leq x < 2.5$) formed. During this time, a decrease of the oxygen content was clearly observed. The changes in surface carbon were similar to that observed near 100 °C. Carbon remained constant after an initial decrease in peak intensity and change in peak shape upon heating. However, annealing at the temperatures < 200 °C, had little effect on Nb_2O at the interface. Figure 4 shows difference spectra. No changes around 203 eV are seen.

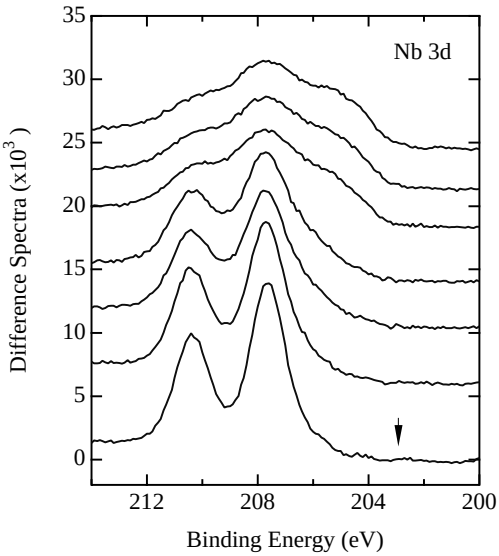

Figure 4: Difference spectra for the sample annealed at 170 °C (Fig. 3). The arrow indicates the binding energy of the Nb_2O Nb-3d peak.

Near 210 °C, Nb_2O_5 disappeared after ~25 h, beyond which oxide conversion continued from a high to low valence state. Annealing affected the interface and more Nb_2O formed. The O-1s peak decreased at a higher rate, which correlated with the oxide conversion, and the C-1s peak remained graphitic. After ~30 h annealing, more than half of the surface carbon reacted with Nb, forming metal carbide. At temperatures between 250 and 300 °C, only Nb_2O remained on the surface, which was stable and inert in vacuum and exhibited a metallic character [12]. The amount of Nb_2O depended on the initial amount of Nb_2O_5

From the data presented in Fig. 3, the reaction rate *k* was estimated for the Nb_2O_5 reduction. Assuming a first-order, reversible reaction, the reduction was described by:

$$-\ln[(A_t - A_c)/(1-A_c)] = kt,$$

where A_t was the area under the Nb_2O_5 peak at *t* and A_c was the area under the Nb_2O_5 peak after completion of the reaction. Both were normalized to the initial area [3]. The results for 170 °C and 210 °C are shown in Fig. 5. A linear relationship was obtained in each case, which satisfied the assumption of reaction kinetics. The slope gives *k*. The *k* value at 210 °C was an order of magnitude larger than that at 170 °C. Using these two data points, E_a ~135 kJ/mole was estimated from the slope of the Arrhenius plot: ln*k* vs *1/T*. To have a more accurate estimate, more data points will be obtained in future studies. Compared to that obtained by King *et al*., this value was smaller. The reason could lie in the fact that the value in [3] was obtained using the O-1s peak, which also included formation of the suboxides while it was calculated only for Nb_2O_5 here. The present result should be more meaningful.

For the data at 100 °C, a change in the *k* value occurred at ~9 h, which might indicate two mechanisms that operated during annealing. The *k* value for the first portion was four times that at 170 °C, while the value for the second portion was much smaller. Relating this to the initial change of the C-1s peak tentatively suggests that the initial changes in the oxides might be brought about by (formation and) desorption of carbon oxide species. This should also exist in the high T data, where the effect might occur in a short time and be averaged out over time. Clearly, more studies are needed to better understand this.

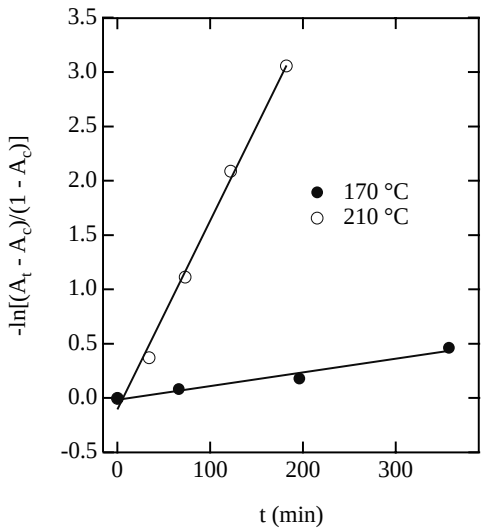

Figure 5: First-order Nb_2O_5 reduction kinetics.

The surface SEYs decreased as a function of annealing temperature and time, indicating that the surface became more conducting. Figure 6 shows the SEYs for the surfaces at the end of heating. A typical as-received surface showed a much higher SEY, σ_{max} ~ 1.8. When the surface was annealed at >250 °C, σ_{max} ~ 1.1 [12].

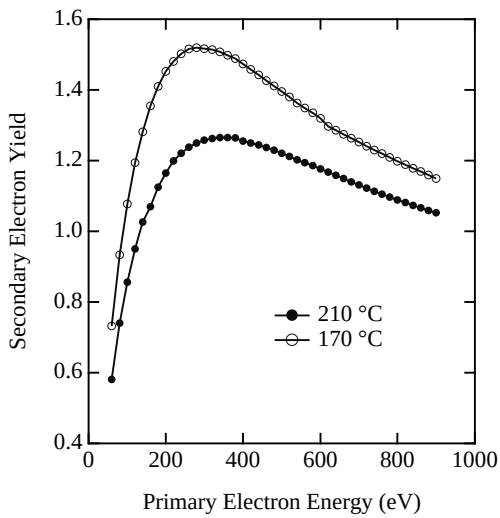

Figure 6: SEYs measured after 170- and 210-°C annealing, respectively.

5. ELECTRON BEAM IRRADIATION

One-keV electrons were used to irradiate the BCP-prepared Nb samples in UHV. The electron current density was < 3 μA/cm^2. Conversion of Nb_2O_5 to NbO_2 has occurred upon electron irradiation, which is consistent with the results reported by Grundner and Halbritter [9]. By XPS and SEY measurements, it was possible to monitor electron-induced surface chemistry as well as damages as a function of electron dose. Figure 7 displayed the SEY peak maximal against electron dose for two samples. The differences were due to the details of the surface chemistry after BCP treatment. However, the shape of the curves was universal, and the slope changed around the same dose regardless of electron current density.

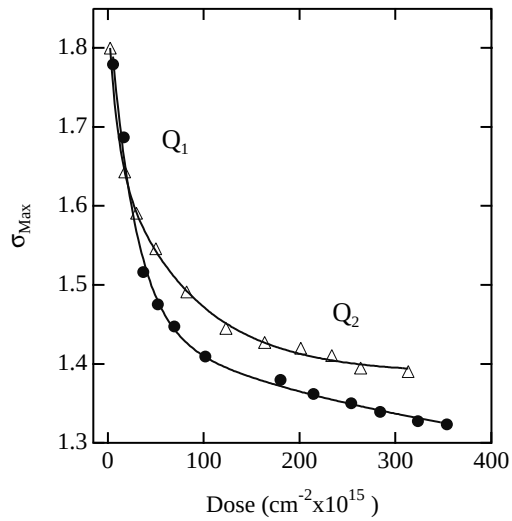

Figure 7: SEYs vs electron dose for two samples.

Each portion of these data was modeled using the first-order rate equation: $\sigma = \sigma_o\, e^{-DQ/q}$ that gave the effective cross section Q for electron-induced change [13]. D is electron dose per cm^2 and q is electron charge. On average, $Q_1 = 4.8\times10^{-18}$ cm^2 and $Q_2 = 2.3\times10^{-19}$ cm^2, respectively, for the first and second portions. Q_1 is a typical value at the lower end of cross sections for dissociative ionization of adsorbed molecules (10^{-16} - 10^{-18} cm^2) [7,13]. In the dose range that contains the Q_1 portion, XPS data (not shown) indicates formation of graphitic carbon upon hydrocarbon decomposition in this dose range. Q_2 is consistent with that obtained by Garwin *et al*. [7] and is associated with electron-induced damage of the oxides. Therefore, the decrease in the SEY of an as-prepared Nb surface appears to be due to both graphitization and oxide damage.

6. CONCLUSIONS

Preliminary results of a study of thermal and electron-beam irradiation effects on the surfaces of Nb used for rf cavity production are presented. A layer of Nb_2O_5 covered the as-prepared Nb surfaces with suboxides interfacing with the Nb metal. Some hydrocarbon species were also found on the surface. Nb_2O was unambiguously determined to exist at the interface to the Nb metal. Oxidation of as-prepared surfaces in air at room temperature was likely to be field assisted.

Heating the samples at temperatures from 100 - 300 ℃ caused reduction of the surface oxide. The reduction rate increased with temperature. Near 100 °C some Nb_2O_5 reduced, and formation of NbO_x ($x < 2.5$) was seen. Near 170 °C, only a little Nb_2O_5 remained after > 70 h. Substantial amounts of NbO_x ($1 \le x < 2.5$) formed. Heating at these temperatures caused hydrocarbon decomposition, leaving graphitic carbon on the surface. It however had no effect on Nb_2O at the interface. At temperatures > 210 °C, Nb_2O_5 completely disappeared, and only Nb_2O remained on the surface that exhibited a metallic character [12]. In addition, more than half of the surface carbon reacted with Nb and formed metal carbide. The analysis of reaction kinetics yielded an activation energy of ~135 kJ/mol for the Nb_2O_5 reduction. These results could be significant for understanding the baking behavior of cavities around 150 °C [1,2].

Under 1-keV electron beam irradiation, surface damage occurred. Changes in the SEY were observed and identified to be due to two causes: surface chemistry change and defect creation in oxides, for which the effective cross section values were estimated, respectively, and were consistent with those found in literature.

7. ACKNOWLEDGMENTS

We would like to thank Mike McDowell for his assistance. Communications with Dr. Lutz Lilji at DESY, Germany and Dr. Bernard Visentin at CEA, France are appreciated.

8. REFERENCES

[1] B. Visentin *et al*., in Proceedings of 9th Workshop on RF Superconductivity, Vol. 1, pp.198 (Santa Fe, 1999).
[2] P. Kneisel *et al*., in Proceedings of 9th Workshop on RF Superconductivity, Vol. 1, pp.328 (Santa Fe, 1999).
[3] B. R. King *et al*., Thin Solid Films 192, 351 (1990).
[4] J. Halbritter, Appl. Phys. A43, 1-28 (1987).
[5] H. Oechsner *et al*., Thin Solid Films 124, 199 (1985)
[6] A. Dacca *et al*., Appl. Surf. Sci. 126, 219 (1998).
[7] E. L. Garwin *et al*., J. Appl. Phys. 61, 1145 (1987).
[8] N. Norman, J. Less Common Metals 4, 124 (1962).
[9] M. Grundner and J. Halbritter, J. Appl. Phys. 51(1), 397 (1980).
[10] N. Cabrera and N. F. Mott, Rep. Prog. Phys. 12, 163 (1948).
[11] R. J. Cvetanovic and Y. Amenoniya, Catal. Rev. Sci. 6, 21 (1972).
[12] Q. Ma and R.A. Rosenberg, in Proceedings of PAC, (Chicago, 2001), in press.
[13] C. G. Pantano and T. E. Madey, Application of Surf. Sci. 7, 115 (1981).